PCCP

Accepted Manuscript

ROYAL SOCIETY OF CHEMISTRY

www.rsc.org/pccp

PCCP

On the Crumpling of Polycrystalline Graphene by Molecular Dynamics Simulation

Journal:	*Physical Chemistry Chemical Physics*
Manuscript ID:	CP-ART-12-2014-005813.R1
Article Type:	Paper
Date Submitted by the Author:	11-Dec-2014
Complete List of Authors:	Becton, Matthew; University of Georgia, College of Engineering Zhang, Liuyang; University of Georgia, College of Engineering Wang, Xianqiao; University of Georgia, College of Engineering

On the Crumpling of Polycrystalline Graphene by Molecular Dynamics Simulation

Matthew Becton[†], Liuyang Zhang[†], and Xianqiao Wang[*†]

College of Engineering, University of Georgia, Athens, GA 30602 USA

Abstract

Crumpled graphene has been emerging as a valuable component for a variety of devices such as supercapacitors or hydrophobic surface coatings due to its geometric change from a 2D to a 3D structure accompanied by changes in its material behavior. As polycrystalline graphene is easier to produce than pristine graphene, certain applications of crumpled graphene may be better suited to polycrystalline graphene. However, the crumpling process of polycrystalline graphene and its relevant mechanical properties remain poorly understood. Here we employ molecular dynamics simulation to model the behavior of polycrystalline graphene under geometric confinement and elucidate the effect of grain size, with a focus on the mechanical stabilizing mechanisms and properties of the crumpled structures in comparison to pristine graphene. Simulation results show that crumpled polycrystalline graphene exhibits a slight negative correlation between average grain size and measured hardness, bulk modulus, and crumpled size. As the size of the grains decreases, the crumpled structures formed are harder and smaller, with sharp edges caused by the grain boundaries. These findings provide evidence towards the feasibility of using polycrystalline graphene in place of pristine graphene in applications involving crumpled carbon structures.

Keywords: Crumpling, Polycrystalline graphene, Molecular Dynamics

Introduction

Since the first laboratory synthesis of graphene in 2003, this 2D carbon material has captured the interest of the scientific community due to its exceptional thermal[1-4], electronic[5, 6], and mechanical[7-9] properties. Due to these outstanding properties, this novel material has demonstrated an exceptional potential in applications such as electronics[10-13], energy storage[14-18], composites[19-23] and biomedicine[24-26]. Due to the profound impact of the utilization of graphene in current and future devices, it is important to find out its properties over a large manifold of potential situations in order to maximize the potential of future development. It is for this reason that not just graphene, but related 2-D carbon materials are tested under a variety of conditions including axial stress, defect formation, doping, wrinkling, and crumpling[8, 20, 27-34]. These studies have shown that chemical and physical alteration to the planar nature of graphene can have surprising and useful benefits to its application in a variety of fields[5, 35, 36]. Of the methods of deformation, perhaps crumpling induces the largest change to a 2-D structure, transforming it from a sheet into a 3-D object while maintaining a large surface area and free volume. When crumpling a piece of paper, the crumpling process endows the material with surprising isotropic compressive strength, and a similar mechanism transforms planar nanomaterials such as graphene and its derivatives[37-39] during the crumpling process as well. The deformation of graphene can strongly affect properties such as diffusion[40] and electrical conductivity[26, 41], and has a notable effect on the performance of graphene-based devices and materials. Crumpled graphene, wherein the 2D material is transformed into a 3D one by a method of mechanically constricting it, has been shown to create a material which exhibits many intriguing properties[29], such as hydrophobicity[42], resilience[43, 44], and electric capacitance[45]. The crumpling effect can be easily achieved via methods such as aerosolization[37, 46, 47], and as such,

given an easily produced source material the crumpled structure can be mass-produced for a wealth of uses. The use of crumpling as a method to rationally alter the properties of graphene and graphene oxide while maintaining surface area has been explored in previous works[29, 39, 44, 46-50], and it is highly worthwhile to investigate the crumpling behavior of 2-D materials similar to graphene as a method of controlled material manufacture.

Towards this end we propose investigating the crumpling process of polycrystalline graphene, or polygraphene. While the techniques for growing graphene have been improved and scaled up, it requires careful oversight and refined techniques to produce graphene in the monocrystalline form[3, 51, 52]. For a large batch of material, it is easier and more cost-effective to produce polygraphene. Polygraphene is created when graphene begins to grow in several places on a substrate, with each grain having a different orientation and thus mismatching when the grains come together to produce a single sheet[53-55]. These grain boundaries weaken the tensile properties of the resulting structure and decrease the electrical and thermal conductivity of graphene, in general making polygraphene less desirable as a source material[6, 56-60]. However, a crumpled structure is not meant for tensile stress, and the nature of its bends and folds are already an impediment to the transport of electricity and heat. In this case, perhaps a cheaper alternative to the production of crumpled pristine graphene structures is the production of crumpled polygraphene structures.

This paper seeks to study and understand the differences and similarities between the crumpled structures of monocrystalline and polycrystalline graphene, to see if crumpled polygraphene is suitable to be used as a cheaper alternative in certain applications, or even if it can be preferable to use polygraphene in some situations. This work will focus on the differences between pristine

graphene and polygraphene during the crumpling process, as well as on any differences between polygraphenes with different grain sizes.

Computational Methods

Molecular dynamics simulations in this work are based on the open source code LAMMPS[61]. Aperiodic boundary conditions are employed to set up the simulation system with minimal self-interference. In order to best capture the behavior of the carbon surfaces we utilize the adaptive intermolecular reactive empirical bond order (AIREBO) potential for intra-graphene carbons as described by Stuart et al.[62] as

$$\boldsymbol{E} = \frac{\mathbf{1}}{\mathbf{2}}\sum_{\boldsymbol{i}}\sum_{\boldsymbol{j}\neq\boldsymbol{i}}\left[\boldsymbol{E}_{\boldsymbol{ij}}^{\boldsymbol{REBO}} + \boldsymbol{E}_{\boldsymbol{ij}}^{\boldsymbol{LJ}} + \sum_{\boldsymbol{k}\neq\boldsymbol{i},\boldsymbol{j}}\sum_{\boldsymbol{l}\neq\boldsymbol{i},\boldsymbol{j},\boldsymbol{k}}\boldsymbol{E}_{\boldsymbol{kijl}}^{\boldsymbol{TORSION}}\right] \quad (1)$$

where the E_{ij}^{REBO} term is the REBO potential published by Brenner et al.[63], shown as

$$\boldsymbol{E}_{\boldsymbol{ij}}^{\boldsymbol{REBO}} = \boldsymbol{V}_{\boldsymbol{ij}}^{\boldsymbol{R}}(\boldsymbol{r}_{\boldsymbol{ij}}) + \boldsymbol{b}_{\boldsymbol{ij}}\boldsymbol{V}_{\boldsymbol{ij}}^{\boldsymbol{A}}(\boldsymbol{r}_{\boldsymbol{ij}}) \quad (2)$$

where V_{ij}^{R} is a repulsive term, V_{ij}^{A} is an attractive term, and b_{ij} is the environmental-dependent bond order term between atoms which activates the attractive term only for bonded atoms. The AIREBO potential is best suited for systems of hydrogen and carbon, rendering the all-carbon system presented here well defined[62]. As the REBO potential only accounts for interactions of atoms within two Angstroms of one another, the AIREBO potential also includes the E^{LJ} term, which is a standard 12-6 Lennard-Jones potential for distances 2 Å $< r <$ cutoff. The cutoff for the LJ term is set here to be 10.2 Å as a good balance between computation speed and accuracy. The AIREBO potential also includes the $E_{kijl}^{TORSION}$ term, which is a four-body potential describing hydrocarbon dihedral angle preference. The AIREBO potential has previously been

used successfully in studying the properties of various carbon allotropes, especially including graphene[64-66].

The simulated sample is a single sheet of polygraphene under a Nose-Hoover thermostat of 1 K with a constant number of atoms and standard velocity-Verlet time integration with timestep of 1fs. The tested samples are square sheets with an edge length of 24 nm. In this work, the initial plane of the nanosheet is considered to be the $x-y$ plane, and perpendicular to the nanosheet is the z direction. Positive z is determined in each sample to be the direction of the first buckling process, as before crumpling the system is symmetric in the z direction. The boundaries are aperiodic so as to prevent self-interference in the sample, and a randomized initial velocity is applied to each atom in accordance with the sample temperature of 1 K, with ensured sum zero linear and angular momenta. The grain sizes (referred to as g) tested in this work are (on average) 2, 3, 4, 6, 8, 12, and "infinite" (pristine graphene) nm. In this manner the number of grains across the sample is an integer ranging from 12 to 1 with each sample having a normally distributed size about the average grain size g; the graphene grains are generated using a Voronoi cell method[67]. After the annealing process the sample is allowed to equilibrate for 400 ps before geometric confinement is applied as shown in Figure 1. The geometric confinement chosen here is spherical, in order to mimic the effect of the aerosol evaporation method of generating crumpled graphene and graphene oxide[38, 47-49, 68]. During geometric confinement the temperature is constrained to 1 K as a constant force is generated spherically around the center of mass of the sample as defined by

$$\boldsymbol{F}(\boldsymbol{r_i}) = -\boldsymbol{K}(\boldsymbol{r_i} - \boldsymbol{R_c})^{\boldsymbol{2}} \tag{3}$$

where K is the force constant equal here to 10 eV/nm^3, r_i is the distance from the i^{th} atom to the center of the confining sphere (which is the same as the center of mass of the polygraphene

sample), and R_c is the radius of confinement. This confining force is normal to the surface of the defined sphere, always repulsive, and is equal to zero when $r < R_c$. At the time when the confinement sphere is generated, R_c is 17.5 nm, larger than the distance to the edge atoms of the sample (17 nm) in order to negate any interference due to the sudden creation of the confining force. As R_c is gradually lessened the sample is forced to crumple to accommodate the reduction in volume, as shown in Figure 1. The relative change of R_c with respect to that at the moment of initiation (R_{c0}) will be referred to as ρ_c, defined explicitly as

$$\boldsymbol{\rho_c = \frac{R_c}{R_{c0}}} \tag{4}$$

The radius of confinement is reduced such that the number of carbon atoms in the final volume is equivalent to the bulk density of graphite (2.267 g/cm^3 or 1.365 u/Å^3 or 113.75 carbon atoms/nm^3), to ensure that the pressure does not cause amorphous collapse or approach the sp^2/sp^3 hybridization transition[69]. For the sample sizes chosen here, this translates to a final R_c which is approximately 20% of R_{c0}.

Results and Discussions

Evolution of Crumpling Process

In order to better compare the crumpling processes of each sample, the general crumpling behavior common to both pristine graphene and polygraphene is studied and denoted. To better understand individual processes which contribute to the final behavior of the crumpled structure, it is useful to take a close look at the evolution of the crumpling process of the nanosheet under spherical confinement. As shown in Figure 1, the square nanosheet is initially flat. As the confining sphere shrinks, the corners of the nanosheet come into contact with it, bending and folding inwards. This bending of the nanosheet strains the C-C bonds, leading to a steady

increase in the potential energy of the system. When two sections of the sheet are forced close enough together they form van der Waals bonds and adhere to each other. Once R_c has reached the targeted value, the confinement is released and there is a decrease in the potential energy as the pressure is released and the structure seeks an equilibrium state, where the structure is held in a partially crumpled structure due to interlayer van der Waals adhesion effects and edge-edge binding. Figure 2 shows a standard example of the crumpling process, using 4 nm polygraphene. It illustrates the folding process of the corners to the inside as the confining sphere shrinks, and shows how the structure maintains its shape after confinement release. As the mass of each sample stays the same while it is the geometry of the sheet which is altered (from a plane to a semi-3D object), to better quantify the change in size of the sample the radius of gyration (R_g) is used in this paper as a way to describe the approximate size of the crumpled nanosheet structure, defined here as

$$\boldsymbol{R_g = \sqrt[2]{\frac{1}{n}\sum |r_i^2 - r_{com}^2|}} \quad (5)$$

Here, n is the number of atoms in the sample, r_i is the position of the i^{th} atom and r_{com} is the position of the center of mass of the nanosheet (which is also the center of the confining sphere). Figure 3 shows the change in the potential energy versus ρ_g for 2 nm polygraphene over the course of the run, ρ_g defined here as the ratio of the current radius of gyration of the sample with respect to the radius of gyration of the initial sample structure R_{g0}:

$$\boldsymbol{\rho_g = \frac{R_g}{R_{g0}}} \quad (6)$$

Snapshots are included in Figure 3 in order to show the evolution of the structure during compression and release. It can be seen that after release the potential energy of the structure is

lower than it was during compression for the same ρ_g, although it neither unfolds completely nor does the potential energy drop back down to where it was before compression began. The same phenomenon can be seen for each polygraphene and also for pristine graphene in Figure 4, which shows the change in ρ_g for each sample. The rate of change of ρ_g as the radius of the confining sphere decreases linearly is particularly noteworthy. After approximately 6 ns, the rate of change of ρ_g changes markedly. This is due to the structure becoming almost spherical as its natural resiliency causes it to conform to the inner side of the confining sphere. After being constrained until ρ_c is 0.20, at which point ρ_g is approximately 0.32 (dependent on the uniquely folded structure), the confining force is released and as such the structure will partially unfold, visualized in Figure 4 as an increase in ρ_g at the end of the simulation. However, the structure never unfolds completely, instead remaining bound by interactions between the edge carbons and, for the polygraphene sheets, interactions between the less-stable atomic bonds along the grain boundaries[39]. In every case, the overall potential energy in the crumpled state is slightly higher than in the initial planar structure. This phenomenon can be explained by the balance between an increase in potential energy in the crumples due to a bending of the atomic bonds, and a lowering of the potential energy from the stabilizing effect of interlayer adhesion[28, 70]. Each nanosheet follows a relatively random folding pattern, although differences in crumpled volume, crumpled radius, and crumpled smoothness exist due to the variable stiffness and self-adhesion behaviors from the difference in grain sizes, as discussed in the following section. Due to these interactions, the final structure is dependent on grain size.

Effects of Grain Size

The focus of this study is a comparison of the crumpling behavior of several grain sizes of polygraphene, and relating them to pristine graphene. As Figure 4 shows, while there is little

variation in size during maximum confinement, the size of each structure after release and equilibration shows a trend wherein smaller grain sizes produce smaller final structures, as the larger aggregate length of the grain boundaries exhibits more of a binding effect on the structure after confinement release. The extremes of this trend are shown by the disparity between 2 nm grain-sized polygraphene which exhibits a final ρ_g of 0.41 and a post-confinement ρ_g change of 0.08, and pristine graphene with a final ρ_g of 0.5, and a post-confinement ρ_g change of 0.19. The pristine graphene expands and increases its relative radius of gyration by more than twice the amount of the smallest grain polycrystalline graphene due to the lack of defects along grain boundaries binding the structure together. Figure 6 shows the change in potential energy of the structure during the crumpling process. As can be seen, the final potential energy is higher than that of the initial structure due to the increase in potential energy due to the bending and stretching of bonds in order to maintain the crumpled structure. While higher in potential energy, the final structure is stabilized in its crumpled form due to self-adhesion and bond interactions of the non-ideally bonded carbon atoms along the edges and grain boundaries of the sample. The increase in potential energy due to total grain boundary length is emphasized by Figure 7, which shows the potential energy at various points during the crumpling process for each grain size. This representation makes it clear that the more grain boundaries in a structure, the higher the overall potential energy during the whole process, even though there is little difference in the change in the potential energy due to crumpling. Upon closer examination, Figure 8 demonstrates the tendency of folds to form along grain boundaries, these defects allowing a natural place for bending of the polygraphene sheet to take place. Due to this, the folding patterns between pristine graphene and polygraphene are markedly different, as can be seen in Figure 9.

Figure 9 shows the structure of grain sizes 2, 4, and 8 nm polygraphene compared with pristine graphene during several points in the crumpling process and after the confinement is released. It can be seen that structures with smaller grains exhibit a more rigid appearance during the crumpling process. As the grain size doubles the number and surface area of the grains is quartered, showing a marked difference in structural response due to crumpling. Pristine graphene tends to create a single surface of smooth bends and folds, but as the number of grain boundaries increases, these boundaries create rigid boundaries which break up the smoothly bending areas such that polygraphene shows an increased resistance to crumpling. To estimate the mechanical durability for applications such as lubrication or kinetic energy mitigation, a referential hardness $\boldsymbol{H}$ for each polygraphene is estimated using the approximation $\approx -\frac{\boldsymbol{dP}}{\boldsymbol{dR_c}}$ [39], where $\boldsymbol{P}$ is the pressure, computed as

$$\boldsymbol{P} = \frac{\boldsymbol{nk_bT}}{\boldsymbol{V}} + \frac{\sum_i^N \boldsymbol{r_i \cdot f_i}}{\boldsymbol{3V}} \quad (7)$$

where n is the number of atoms, k_b is Boltzmann's constant, T is the temperature, and f_i is the force felt by the ith atom. To estimate H, the 20 ps linear sections at the final stage of crumpling as can be seen in Figure 10 are used as a basis. To more readily exhibit the change in pressure during the final stages of crumpling, the pressure for each grain size at several key points during the process are chosen and exhibited in Figure 11. It is clear to see that the pressure is very similar for each type of polygraphene during most of the crumpling process, only showing clear differentiation at the final step when R_c is minimum and the pressure is maximum. The bulk modulus of an isotropic material is a measurement of a material's change in volume under uniform pressure, useful to know for high temperature- and pressure-capable materials such as pure carbon structures, which can be used in suitable extreme environments. For the calculation

of the hardness and the bulk modulus B, the entire crumpled structure as a whole is considered to be on average an isotropic 3-dimensional structure, as after crumpling the sample achieves a randomized folded 3-D structure which can best be approximated as isotropic. Taking the shape of a 2-D object which becomes 3-D through "crumpling", that is, randomized folding, to be isotropic has been done successfully before previously[39]. While there is a rough correlation between hardness and bulk modulus, unlike hardness, bulk modulus is a material property which is precisely defined; it can be determined by using the formula

$$\boldsymbol{B} = -\boldsymbol{V}\frac{\boldsymbol{dP}}{\boldsymbol{dV}} \quad (8)$$

where V is the volume of the structure. The estimated H and calculated B of each grain size of polygraphene averaged over three runs is presented in Figure 12, and expectedly these structures have a much lower bulk modulus than that of graphite (≈ 34 GPa), as these structures are not flat layered sheets like graphite, and as such have the flexible ability to respond to environmental stresses without brittle rupture. It can be seen that as the grain size shrinks, the hardness and bulk modulus of the sample increases. This can be explained by the increased number of defects for samples with smaller grain sizes, as each grain boundary can be considered a pseudo-linear collection of defects, leading to increased stiffness when compared to larger grain sizes. Pristine graphene being the logically largest grain size, its behavior during crumpling as seen in Figure 9 exhibits smooth curves as it collapses, whereas the structures with grain boundaries tend to crease sharply along these boundaries, creating sharply angled crumples which serve to increase the bulk modulus during heavy compression. This naturally leads to the conclusion that the properties of crumpled polygraphene heavily depend on the size and number of grains of the sample, with smaller grain sizes leading to smaller, harder isotropic structures.

Conclusions

In summary, we have performed molecular dynamics simulation to investigate confinement-induced crumpling of nanosheets of polycrystalline graphene, in order to determine the differences between pristine graphene and polygraphene and also to determine the effect of grain size on the process. It was shown that while there are similarities during the crumpling process, the properties of the final structure generated are dependent on the size of the grains of the sample. To be specific, samples with smaller grains tended towards smaller final structures, with relatively higher hardness and bulk modulus than the samples with larger grains. From this, we can conclude that generated crumpled polygraphene may in fact be more useful for certain applications, as crumpling polygraphene generates harder, denser crumpled structures; the properties can be more finely tuned due to the grain size of the polygraphene. The fundamental findings in this paper provide a promising platform for quantitatively transforming 2-D materials into 3-D isotropic nanoparticles with nonconventional properties and also can serve as a guideline to design novel carbon-based nanomaterials and nanodevices.

Author information

*Corresponding author: Xianqiao Wang

Email: xqwang@uga.edu.

† Present address: College of Engineering, University of Georgia, Athens, Georgia 30606, USA

Competing financial interests: The authors declare no competing financial interests.

Acknowledgements

The authors acknowledge support from the University of Georgia (UGA) Research Foundation. Calculations are performed at the UGA Advanced Computing Resource Centre.

References

1. S. Subrina and D. Kotchetkov, *J Nanoelectron Optoe*, 2008, **3**, 249-269.
2. V. Varshney, S. S. Patnaik, A. K. Roy, G. Froudakis and B. L. Farmer, *Acs Nano*, 2010, **4**, 1153-1161.
3. A. V. Eletskii, I. M. Iskandarova, A. A. Knizhnik and D. N. Krasikov, *Phys-Usp+*, 2011, **54**, 227-258.
4. B. Liu, C. D. Reddy, J. W. Jiang, J. A. Baimova, S. V. Dmitriev, A. A. Nazarov and K. Zhou, *Appl Phys Lett*, 2012, **101**, 211909
5. V. M. Pereira, A. H. C. Neto, H. Y. Liang and L. Mahadevan, *Phys Rev Lett*, 2010, **105**, 156603.
6. O. V. Yazyev and S. G. Louie, *Nature Materials*, 2010, **9**, 806-809.
7. A. Politano, A. R. Marino, D. Campi, D. Farias, R. Miranda and G. Chiarello, *Carbon*, 2012, **50**, 4903-4910.
8. A. Sakhaee-Pour, *Comp Mater Sci*, 2009, **45**, 266-270.
9. S. Koch, D. Stradi, E. Gnecco, S. Barja, S. Kawai, C. Diaz, M. Alcami, F. Martin, A. L. V. de Parga, R. Miranda, T. Glatzel and E. Meyer, *Acs Nano*, 2013, **7**, 2927-2934.
10. P. Blake, P. D. Brimicombe and R. R. Nair, *Nano Lett*, 2008, **8**, 1704-1708.
11. V. Yong and J. M. Tour, *Small*, 2010, **6**, 313-318.
12. C. Jeong, P. Nair, M. Khan, M. Lundstrom and M. A. Alam, *Nano Lett*, 2011, **11**, 5020-5025.
13. M. Y. Liao and Y. Koide, *Crit Rev Solid State*, 2011, **36**, 66-101.
14. S. Goler, C. Coletti, V. Tozzini, V. Piazza, T. Mashoff, F. Beltram, V. Pellegrini and S. Heun, *J Phys Chem C*, 2013, **117**, 11506-11513.
15. V. Tozzini and V. Pellegrini, *Phys Chem Chem Phys*, 2013, **15**, 80-89.
16. D. Deng and J. Y. Lee, *Chem Mater*, 2007, **19**, 4198-4204.
17. Y. F. Li, Z. Zhou, P. W. Shen and Z. F. Chen, *Chem Commun*, 2010, **46**, 3672-3674.
18. A. Politano and G. Chiarello, *Carbon*, 2013, **61**, 412-417.
19. Z. P. Song, T. Xu, M. L. Gordin, Y. B. Jiang, I. T. Bae, Q. F. Xiao, H. Zhan, J. Liu and D. H. Wang, *Nano Lett*, 2012, **12**, 2205-2211.
20. M. A. Rafiee, J. Rafiee, I. Srivastava, Z. Wang, H. H. Song, Z. Z. Yu and N. Koratkar, *Small*, 2010, **6**, 179-183.
21. D. Konatham, K. N. D. Bui, D. V. Papavassiliou and A. Striolo, *Mol Phys*, 2011, **109**, 97-111.
22. V. Alzari, V. Sanna, S. Biccai, T. Caruso, A. Politano, N. Scaramuzza, M. Sechi, D. Nuvoli, R. Sanna and A. Mariani, *Compos Part B-Eng*, 2014, **60**, 29-35.
23. H. Kim, A. A. Abdala and C. W. Macosko, *Macromolecules*, 2010, **43**, 6515-6530.
24. Y. J. Hu, J. A. Jin, H. Zhang, P. Wu and C. X. Cai, *Acta Phys-Chim Sin*, 2010, **26**, 2073-2086.
25. C. A. Merchant, K. Healy, M. Wanunu, V. Ray, N. Peterman, J. Bartel, M. D. Fischbein, K. Venta, Z. T. Luo, A. T. C. Johnson and M. Drndic, *Nano Lett*, 2010, **10**, 2915-2921.
26. R. Kempaiah, A. Chung and V. Maheshwari, *Acs Nano*, 2011, **5**, 6025-6031.
27. Y. F. Li, D. Datta, Z. H. Li and V. B. Shenoy, *Comp Mater Sci*, 2014, **83**, 212-216.
28. X. H. Meng, M. Li, Z. Kang, X. P. Zhang and J. L. Xiao, *J Phys D Appl Phys*, 2013, **46**, 055308.
29. J. R. Zang, S.; Pugno, N.; Wang, Q.; Tu, Q.; Buehler, M.; Zhao, X., *Nat Mater*, 2013, **12**, 321-325.
30. V. R. Coluci, D. S. Galvao and R. H. Baughman, *J Chem Phys*, 2004, **121**, 3228-3237.
31. J. A. Baimova, S. V. Dmitriev, K. Zhou and A. V. Savin, *Phys Rev B*, 2012, **86**, 035427.
32. J. A. Baimova, S. V. Dmitriev and K. Zhou, *Phys Status Solidi B*, 2012, **249**, 1393-1398.
33. X. Chen, L. Zhang, Y. Zhao, X. Wang and C. Ke, *J Appl Phys*, 2014, **116**, 164301.
34. M. Becton, L. Y. Zhang and X. Q. Wang, *Chem Phys Lett*, 2013, **584**, 135-141.
35. K. Kim, Z. Lee, B. D. Malone, K. T. Chan, B. Alemán, W. Regan, W. Gannett, M. F. Crommie, M. L. Cohen and A. Zettl, *Phys Rev B*, 2011, **83**, 245433.

36. S. Ladak, J. M. Ball, D. Moseley, G. Eda, W. R. Branford, M. Chhowalla, T. D. Anthopoulos and L. F. Cohen, *Carbon*, 2013, **64**, 35-44.
37. J. Y. Luo, H. D. Jang, T. Sun, L. Xiao, Z. He, A. P. Katsoulidis, M. G. Kanatzidis, J. M. Gibson and J. X. Huang, *Acs Nano*, 2011, **5**, 8943-8949.
38. F. Guo, M. Creighton, Y. T. Chen, R. Hurt and I. Kulaots, *Carbon*, 2014, **66**, 476-484.
39. C. Chang, Z. G. Song, J. Lin and Z. P. Xu, *Rsc Adv*, 2013, **3**, 2720-2726.
40. S. Jungthawan, P. Reunchan and S. Limpijumnong, *Carbon*, 2013, **54**, 359-364.
41. B. D. Briggs, B. Nagabhirava, G. Rao, R. Geer, H. Y. Gao, Y. Xu and B. Yu, *Appl Phys Lett*, 2010, **97**, 223102.
42. Z. X. Chen, L. Dong, D. Yang and H. B. Lu, *Adv Mater*, 2013, **25**, 5352-5359.
43. C. Hui, Y. Zhang, L. Zhang, R. J. Sun and F. Liu, *J Appl Phys*, 2013, **114**, 163512.
44. O. C. Compton, S. Kim, C. Pierre, J. M. Torkelson and S. T. Nguyen, *Adv Mater*, 2010, **22**, 4759-+.
45. S. L. Zhang and N. Pan, *J Mater Chem A*, 2013, **1**, 7957-7962.
46. S. Mao, Z. H. Wen, H. Kim, G. H. Lu, P. Hurley and J. H. Chen, *Acs Nano*, 2012, **6**, 7505-7513.
47. W. N. Wang, Y. Jiang and P. Biswas, *J Phys Chem Lett*, 2012, **3**, 3228-3233.
48. X. F. Ma, M. R. Zachariah and C. D. Zangmeister, *Nano Lett*, 2012, **12**, 486-489.
49. X. F. Ma, M. R. Zachariah and C. D. Zangmeister, *J Phys Chem C*, 2013, **117**, 3185-3191.
50. S. W. Cranford and M. J. Buehler, *Phys Rev B*, 2011, **84**, 205451.
51. V. Yong and H. T. Hahn, *Crystengcomm*, 2011, **13**, 6933-6936.
52. Q. K. Yu, L. A. Jauregui, W. Wu, R. Colby, J. F. Tian, Z. H. Su, H. L. Cao, Z. H. Liu, D. Pandey, D. G. Wei, T. F. Chung, P. Peng, N. P. Guisinger, E. A. Stach, J. M. Bao, S. S. Pei and Y. P. Chen, *Nature Materials*, 2011, **10**, 443-449.
53. J. Y. Chen, Y. G. Wen, Y. L. Guo, B. Wu, L. P. Huang, Y. Z. Xue, D. C. Geng, D. Wang, G. Yu and Y. Q. Liu, *J Am Chem Soc*, 2011, **133**, 17548-17551.
54. X. S. Li, C. W. Magnuson, A. Venugopal, J. H. An, J. W. Suk, B. Y. Han, M. Borysiak, W. W. Cai, A. Velamakanni, Y. W. Zhu, L. F. Fu, E. M. Vogel, E. Voelkl, L. Colombo and R. S. Ruoff, *Nano Lett*, 2010, **10**, 4328-4334.
55. D. Rhinow, N. E. Weber and A. Turchanin, *J Phys Chem C*, 2012, **116**, 12295-12303.
56. L. A. Jauregui, H. L. Cao, W. Wu, Q. K. Yu and Y. P. Chen, *Solid State Commun*, 2011, **151**, 1100-1104.
57. C. Jasiukiewicz, T. Paszkiewicz and S. Wolski, *Phys Status Solidi B*, 2010, **247**, 1201-1206.
58. A. Bagri, S. P. Kim, R. S. Ruoff and V. B. Shenoy, *Nano Lett*, 2011, **11**, 3917-3921.
59. P. Y. Huang, C. S. Ruiz-Vargas, A. M. van der Zande, W. S. Whitney, M. P. Levendorf, J. W. Kevek, S. Garg, J. S. Alden, C. J. Hustedt, Y. Zhu, J. Park, P. L. McEuen and D. A. Muller, *Nature*, 2011, **469**, 389–392.
60. A. Cao and J. M. Qu, *J Appl Phys*, 2012, **112**, 043519.
61. S. Plimpton, *J Comput Phys*, 1995, **117**, 1-19.
62. S. J. Stuart, A. B. Tutein and J. A. Harrison, *J Chem Phys*, 2000, **112**, 6472-6486.
63. D. W. Brenner, O. A. Shenderova, J. A. Harrison, S. J. Stuart, B. Ni and S. B. Sinnott, *J Phys-Condens Mat*, 2002, **14**, 783-802.
64. M. Becton and X. Q. Wang, *J Chem Theory Comput*, 2014, **10**, 722-730.
65. M. Becton, L. Y. Zhang and X. Q. Wang, *Phys Chem Chem Phys*, 2014, **16**, 18233-18240.
66. S. Zhu and T. Li, *Journal of Physics D: Applied Physics*, 2013, **46**, 075301.
67. N. N. Li, Z. D. Sha, Q. X. Pei and Y. W. Zhang, *J Phys Chem C*, 2014, **118**, 13769-13774.
68. N. Patra, B. Y. Wang and P. Kral, *Nano Lett*, 2010, **239**, 3766-3771.
69. H. W. Day, *Am Mineral*, 2012, **97**, 52-62.
70. S. Cranford, D. Sen and M. J. Buehler, *Appl Phys Lett*, 2009, **95**, 123121.

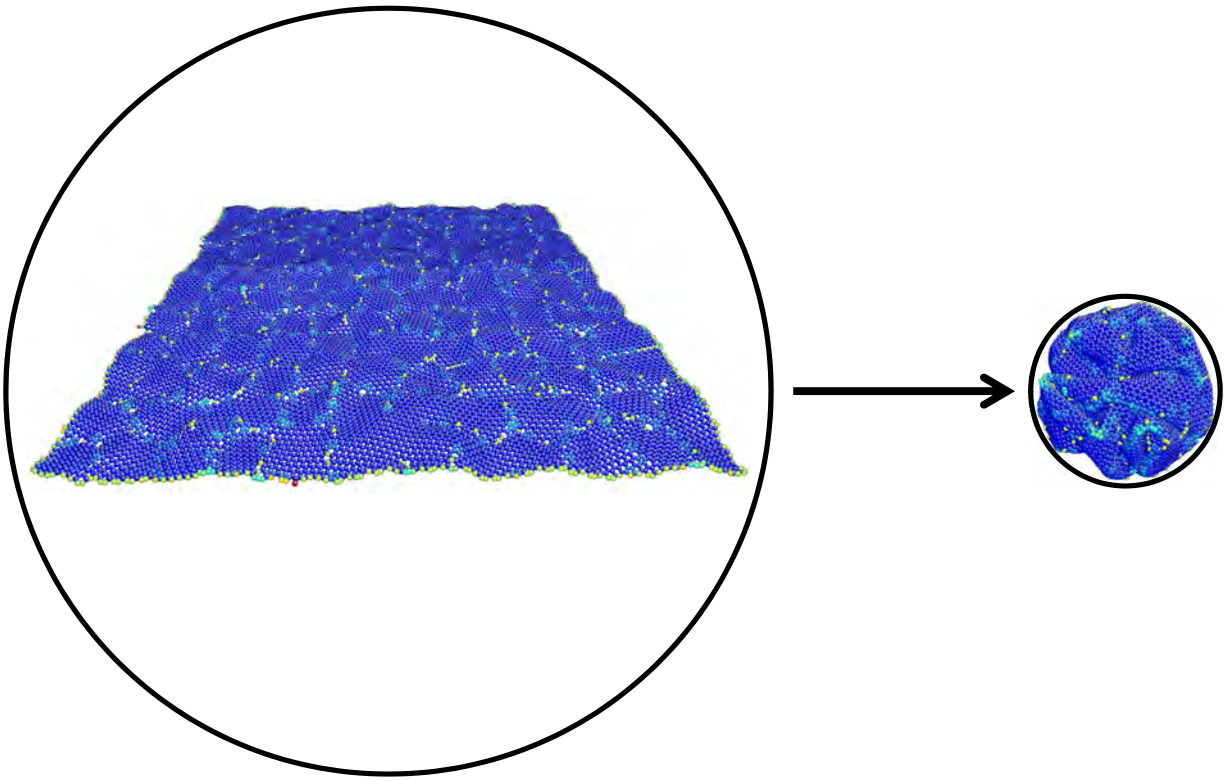

Figure 1: Setup showing polygraphene within the confinement boundary as $\boldsymbol{R_c}$ decreases from the initial state ($\boldsymbol{R_c = 17.5}$ nm) to the final state ($\boldsymbol{R_c = 3.6}$ nm).

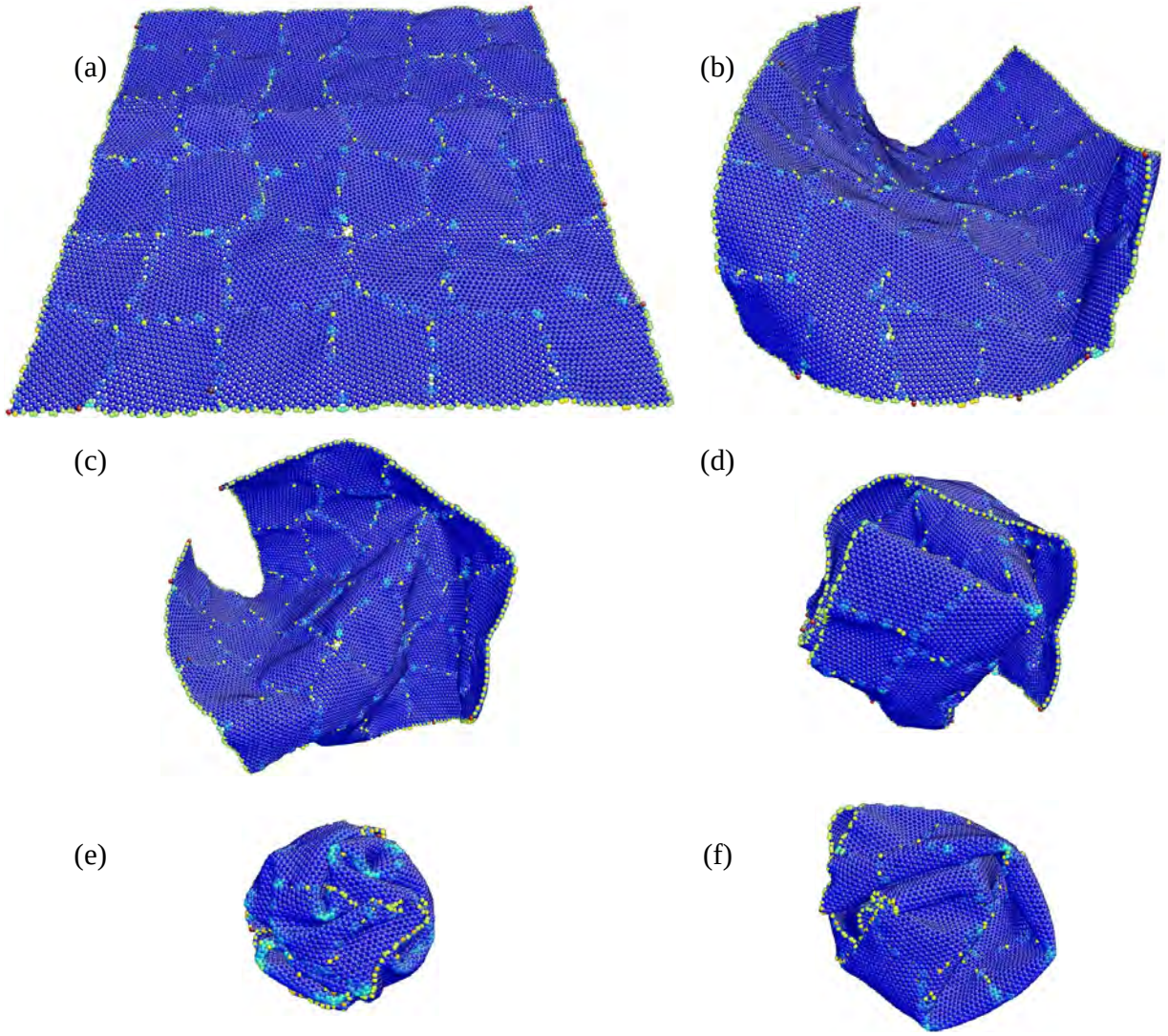

Figure 2: Evolution of the crumpling process: (a) before crumpling, (b) folding of corners, (c) interior folding, (d) self-contact, (e) maximum confinement, and (f) stable state after release and equilibration. The polygraphene portrayed here is the 4 nm grain size.

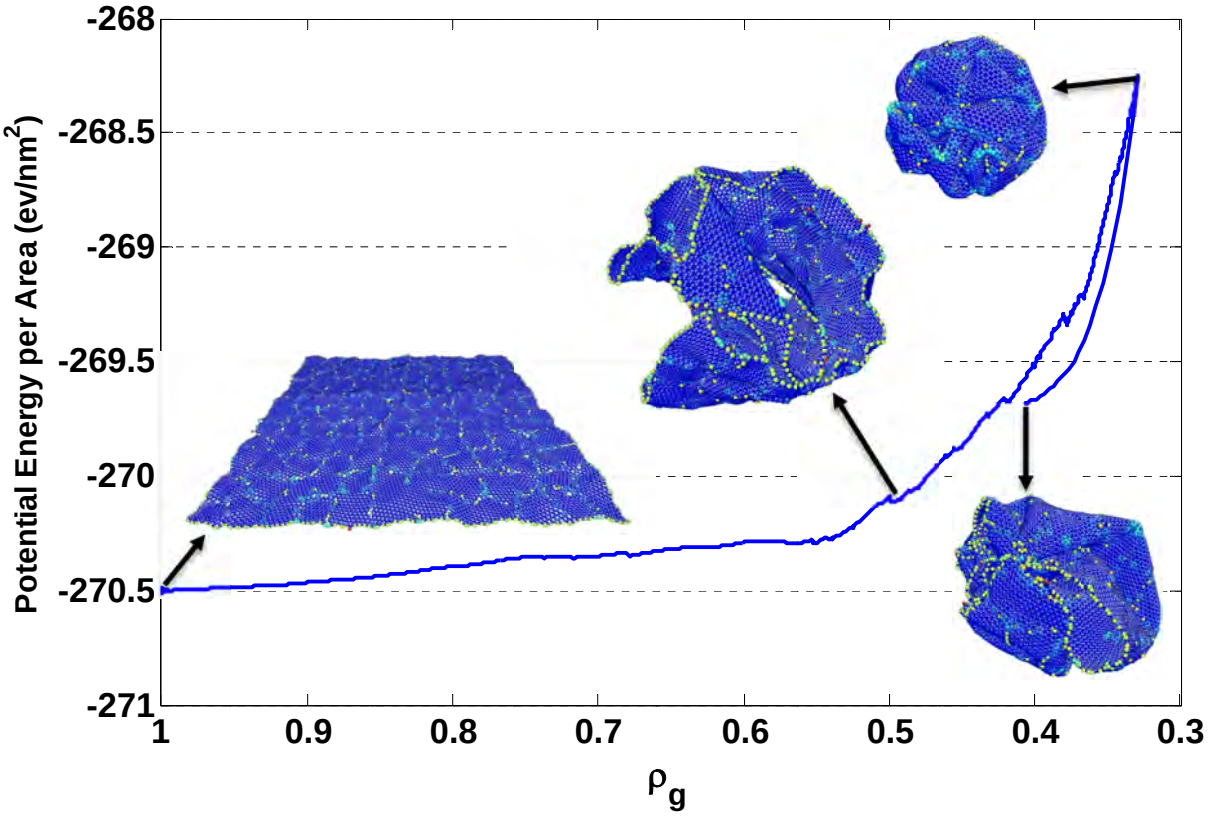

Figure 3: Evolution of potential energy per area as a function of the radius of gyration for 2 nm polygraphene.

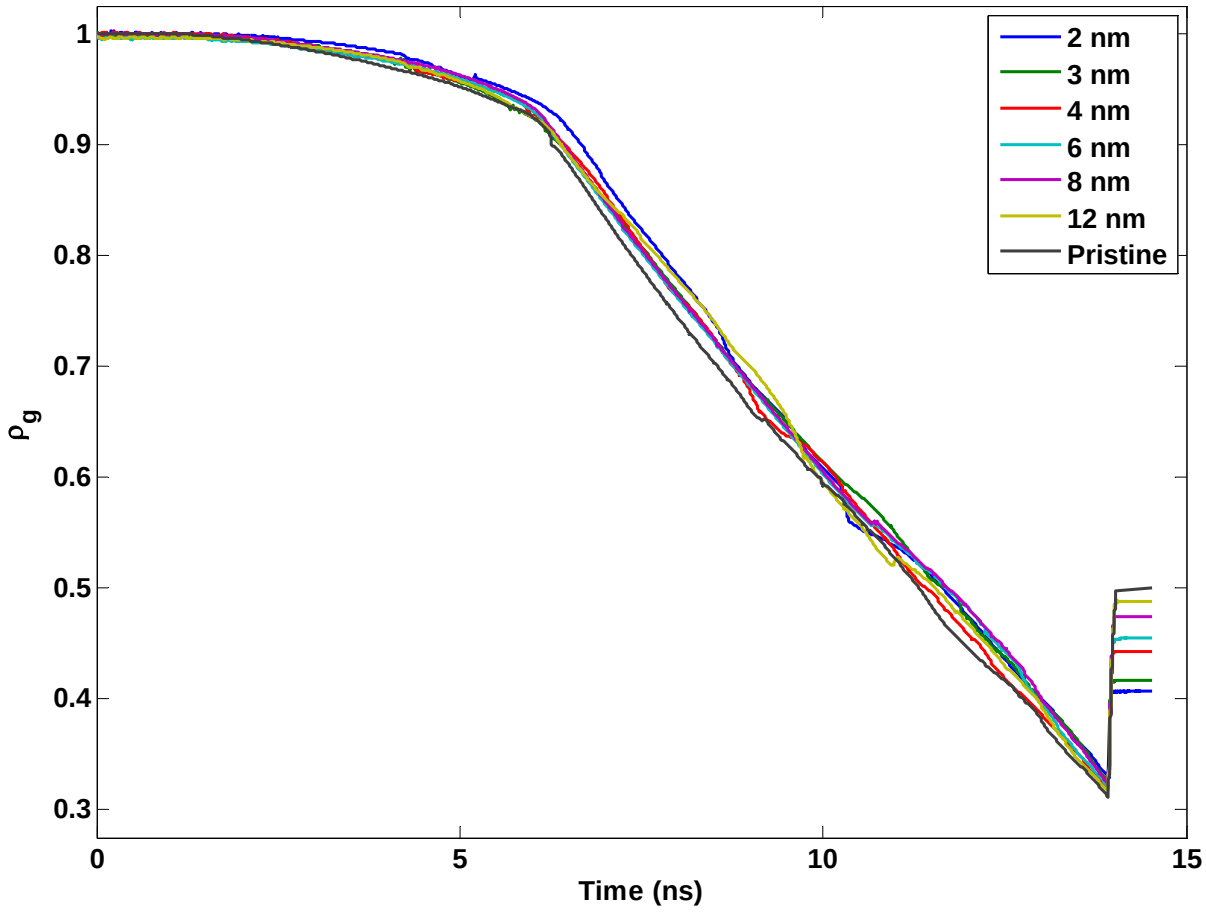

Figure 4: Change in the radius of gyration ratio of each structure.

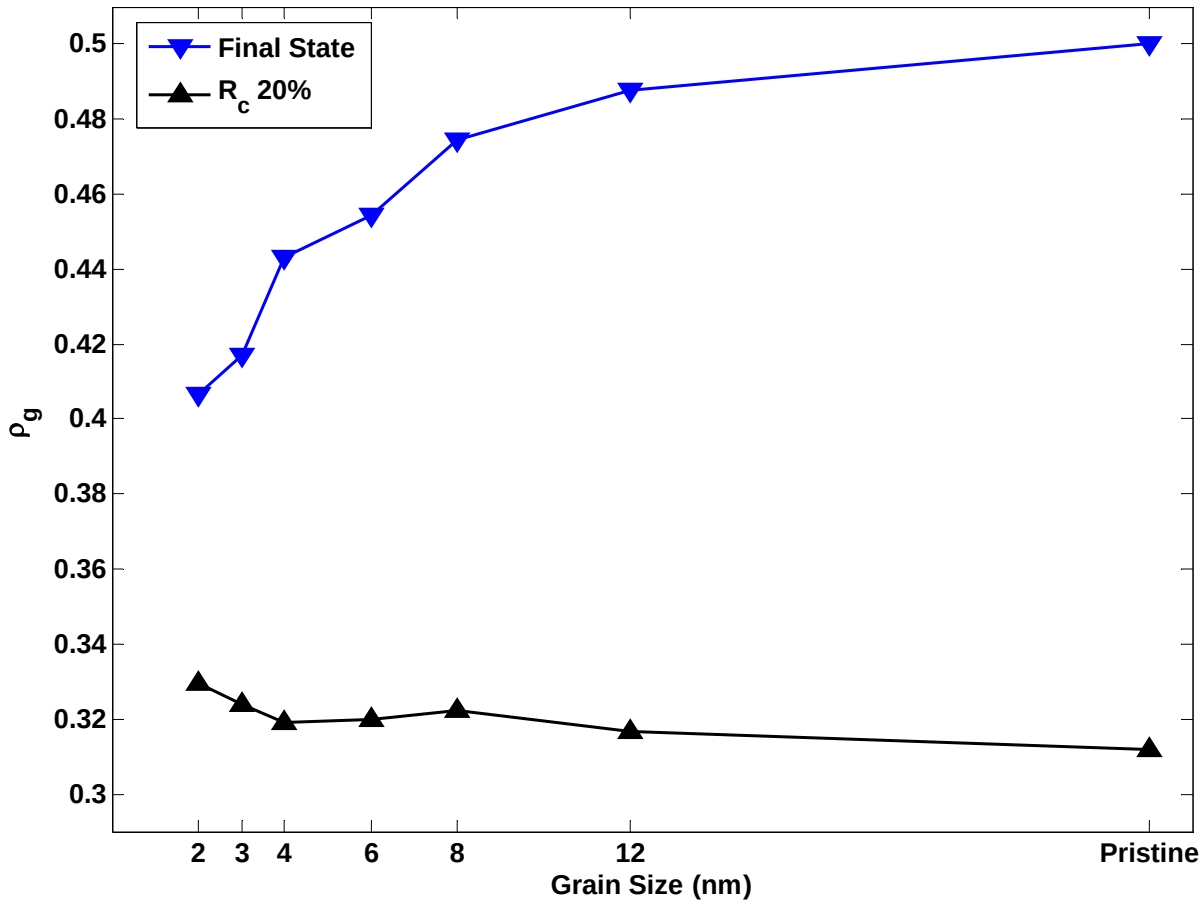

Figure 5: Minimum and final ρ_g for each grain size.

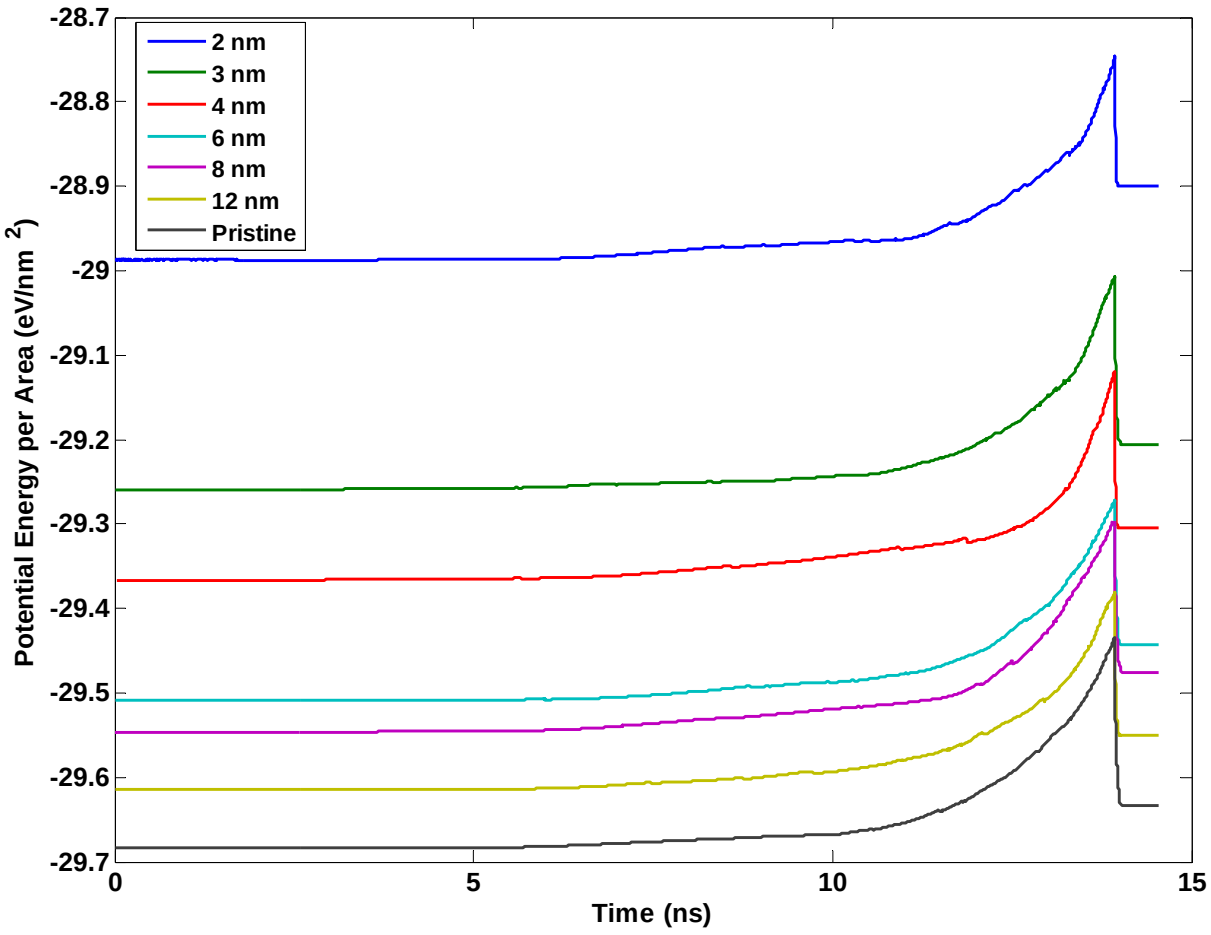

Figure 6: Potential energy of the structure versus time, in order to compare the effect of grain boundaries on the initial and final structures.

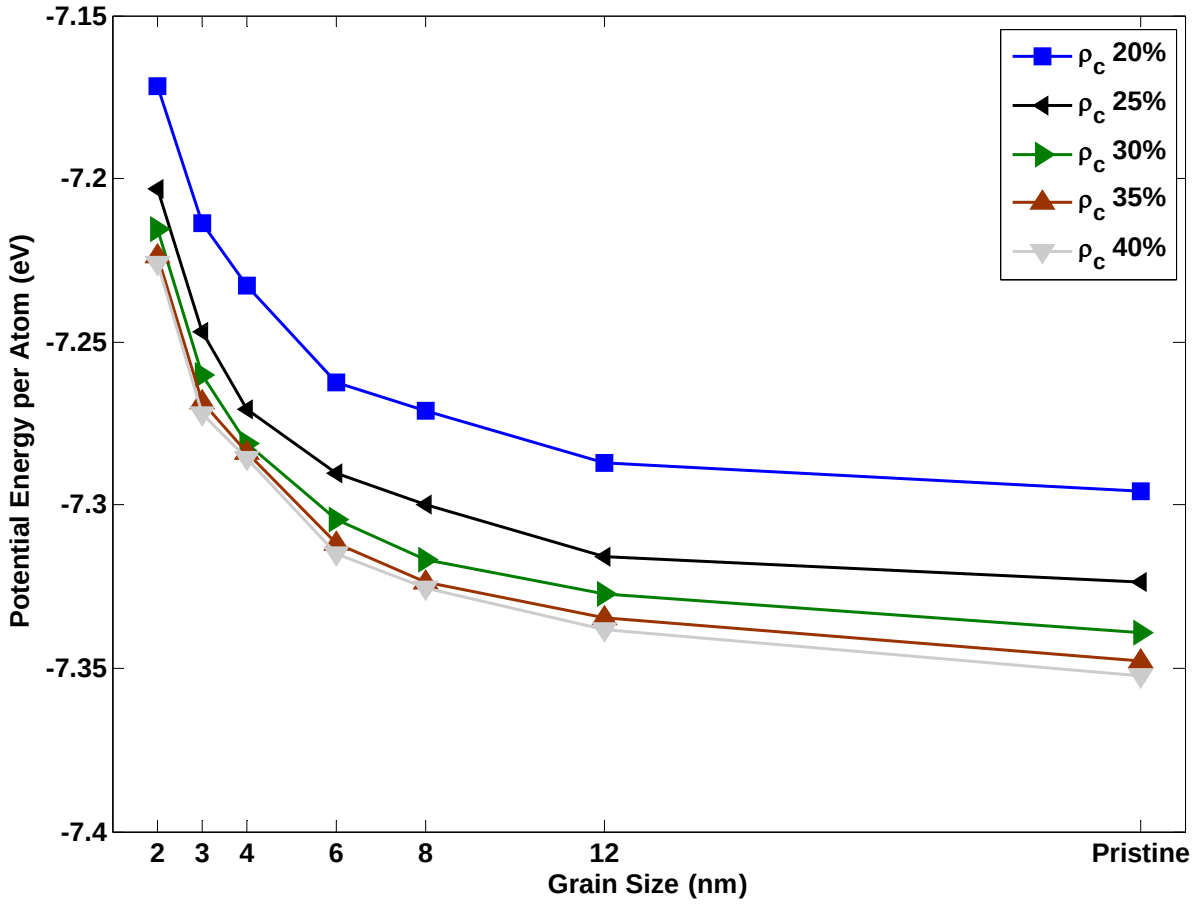

Figure 7: Potential energy as a function of grain size for different values of ρ_c.

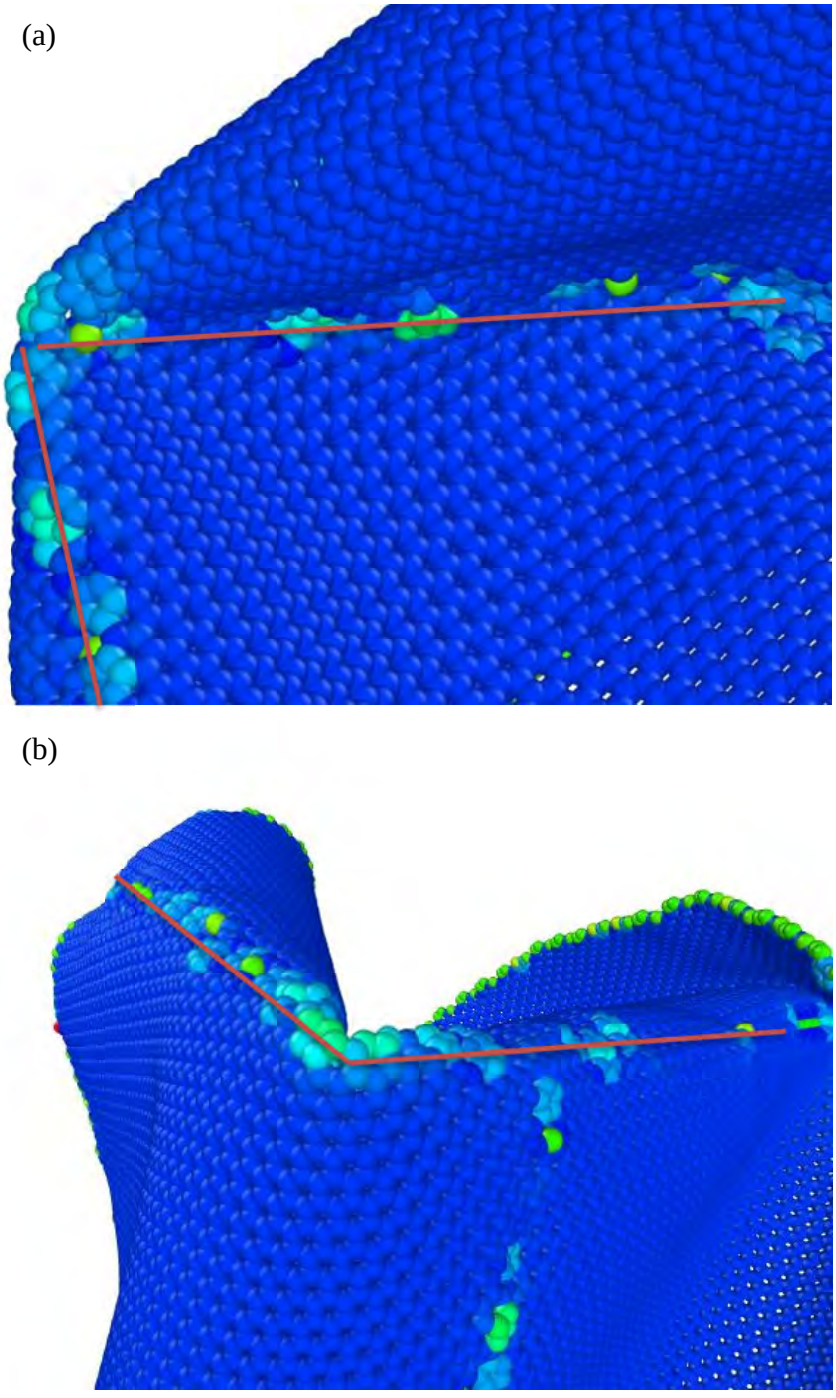

Figure 8: Folding along grain boundaries for (a) 8 nm and (b) 12 nm polygraphene. The red lines are to accentuate the grain boundaries in question.

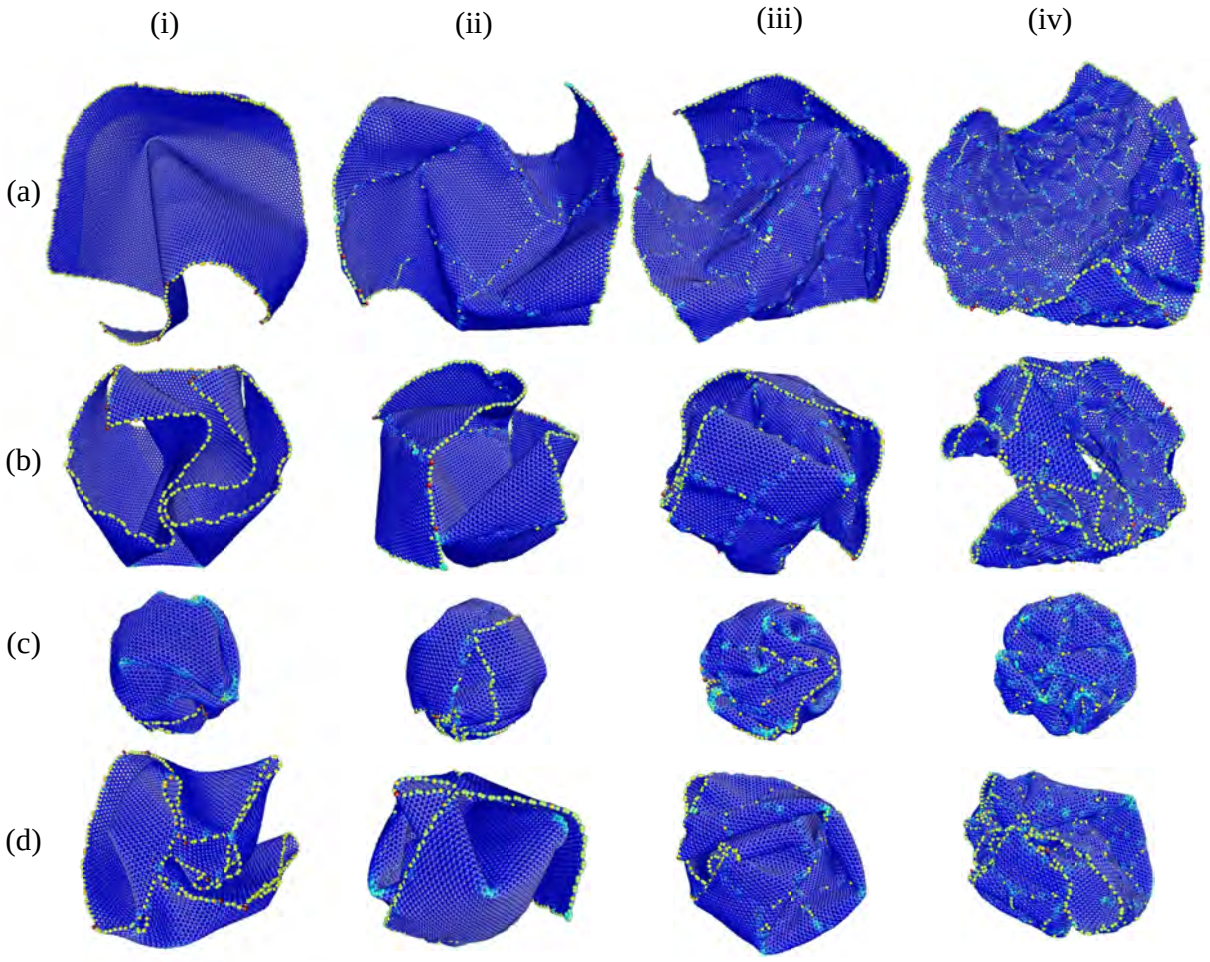

Figure 9: Comparison of the structures for each grain size of polygraphene during several points in the crumpling process: (a) interior folding, (b) self-contact, (c) maximum confinement, and (d) released and equilibrated. From left to right the structures are (i) pristine graphene, (ii) 8 nm grain size, (iii) 4 nm grain size, and (iv) 2 nm grain size.

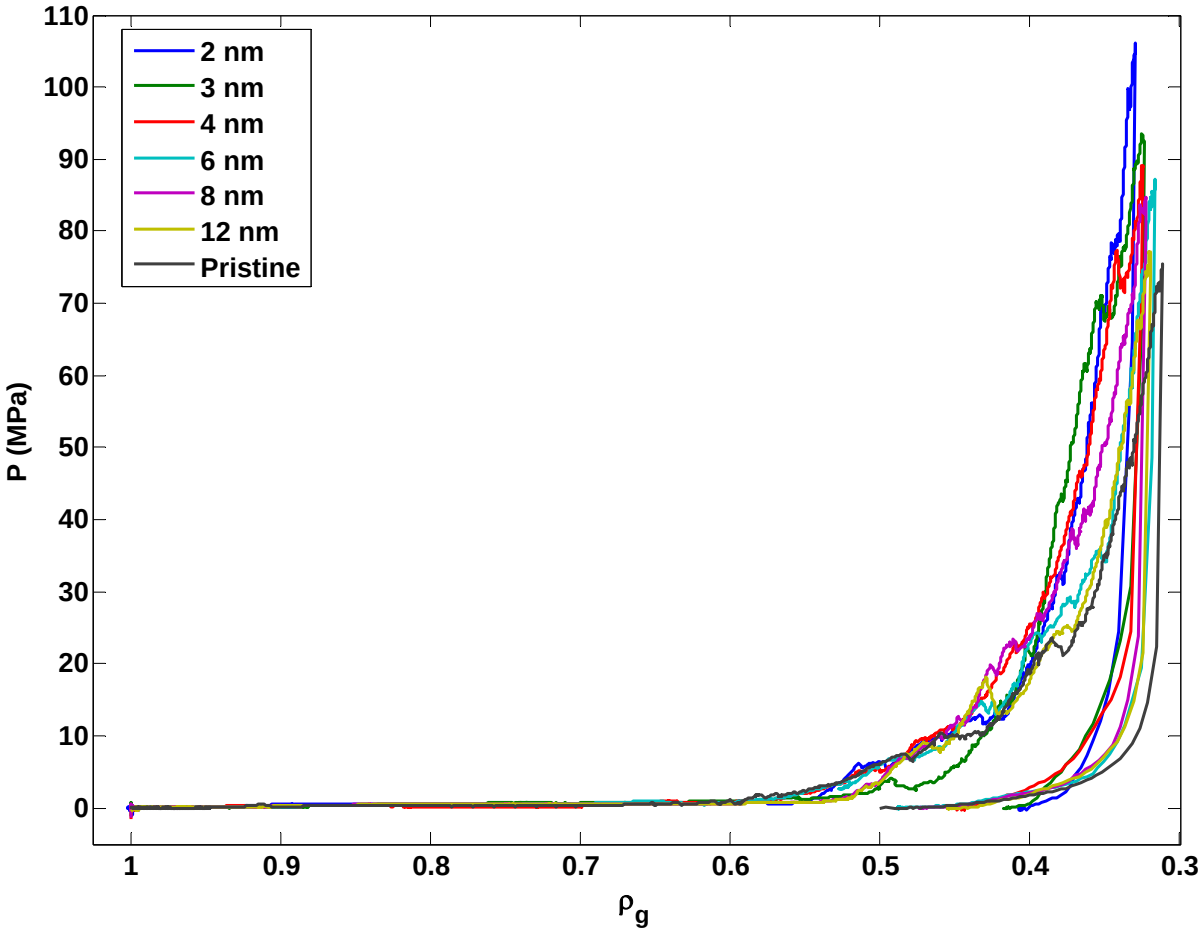

Figure 10: Change in pressure during the crumpling process as a function of $\boldsymbol{\rho_g}$.

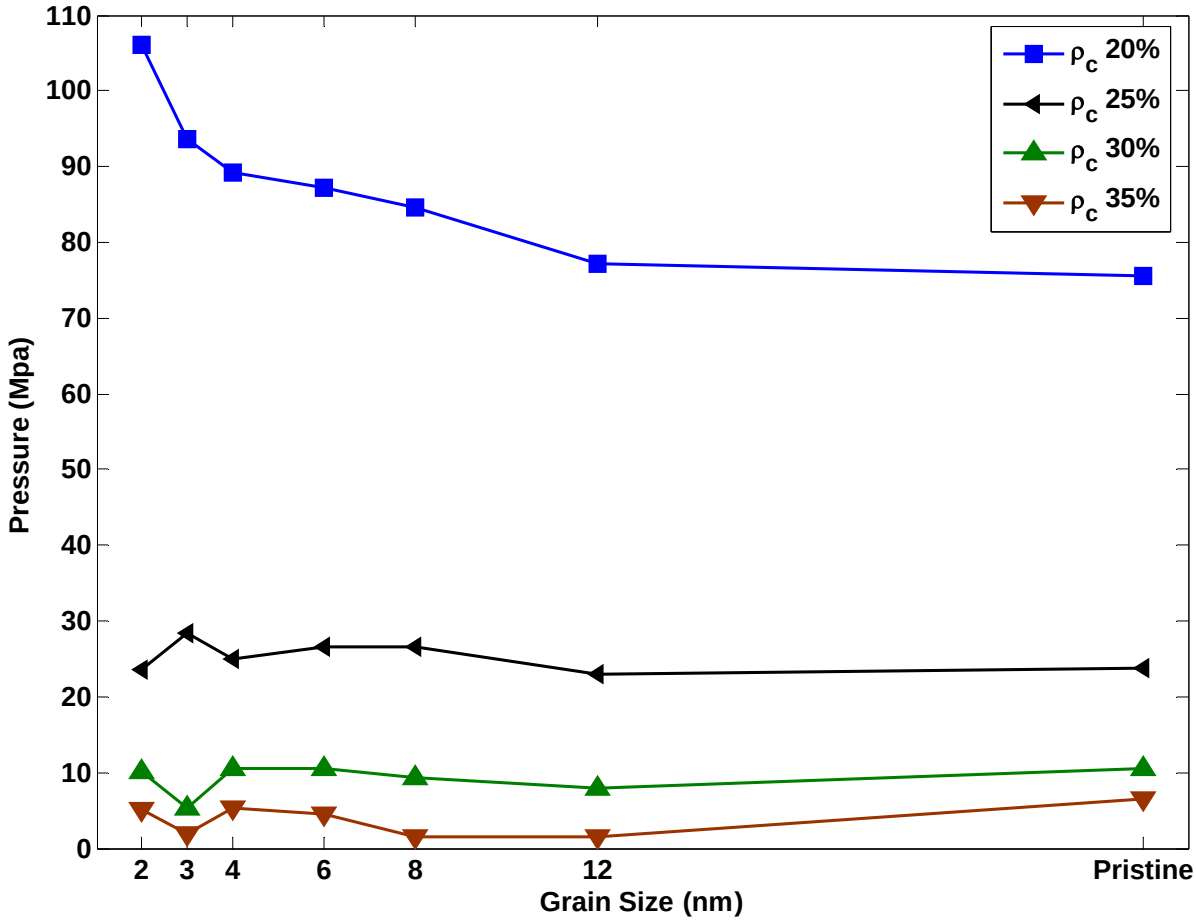

Figure 11: Pressure as a function of grain size at different values of ρ_c.

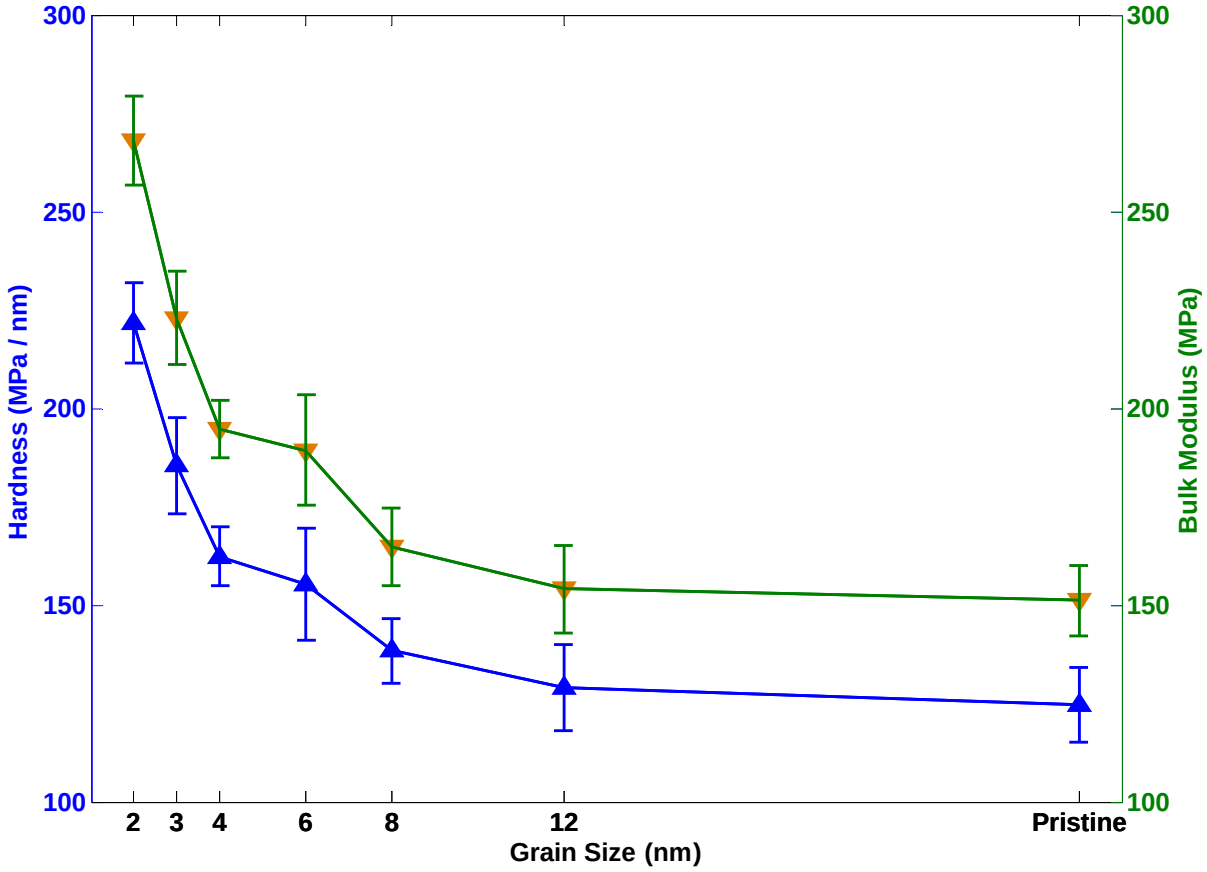

Figure 12: Hardness and bulk modulus of the crumpled structures by grain size.